EVOLUTIONARY BIOLOGY

The hypothalamus predates the origin of vertebrates

Laurence A. Lemaire[1†], Chen Cao[1†], Peter H. Yoon[2‡], Juanjuan Long[1§], Michael Levine[1,2*]

The hypothalamus coordinates neuroendocrine functions in vertebrates. To explore its evolutionary origin, we describe integrated transcriptome/connectome brain maps for swimming tadpoles of *Ciona*, which serves as an approximation of the ancestral proto-vertebrate. This map features several cell types related to different regions of the vertebrate hypothalamus, including the mammillary nucleus, the arcuate nucleus, and magnocellular neurons. Coronet cells express melanopsin and share additional properties with the saccus vasculosus, a specialized region of the hypothalamus that mediates photoperiodism in nontropical fishes. Comparative transcriptome analyses identified orthologous cell types for mechanosensory switch neurons, and *VP*$^+$ and *VPR*$^+$ relay neurons in different regions of the mouse hypothalamus. These observations provide evidence that the hypothalamus predates the evolution of the vertebrate brain. We discuss the possibility that switch neurons, coronet cells, and *FoxP*$^+$/*VPR*$^+$ relay neurons comprise a behavioral circuit that helps trigger metamorphosis of *Ciona* larvae in response to twilight.

INTRODUCTION

The evolution of the vertebrate head is linked to the advent of several key innovations such as neural crest and cranial placodes. The closest living relatives of vertebrates, the tunicates, have been shown to contain sensory neurons that are related to derivatives of both tissues (*1*–*5*). However, less is known about the evolutionary origin of the "crown and summit" of animal innovations: the vertebrate brain. In this study, we use an extensive single-cell transcriptome fate map of the *Ciona* tadpole to characterize the neural cell types comprising its simple brain, or sensory vesicle (*6*).

The sensory vesicle of the *Ciona* tadpole is composed of only 215 neural cells including 143 neurons (*7*, *8*). It is primarily responsible for relaying sensory information, such as light, gravity, and mechanical cues, to the motor ganglion, which controls the rapid swimming strokes of the tadpole tail. The extreme simplicity of the *Ciona* central nervous system (CNS) has facilitated the elucidation of detailed lineage maps and the first comprehensive connectome of a chordate (*7*). Here, we attempt to incorporate the synaptic connectome, along with detailed single-cell transcriptome atlases, to explore the evolutionary origins of the vertebrate brain, particularly the hypothalamus.

The hypothalamus has long been considered to be an "ancient" region of the vertebrate brain. It is found in all vertebrates, from jawless fishes to humans (*9*–*11*). A homologous area is also thought to occur in invertebrate chordates such as cephalochordates (*12*). The hypothalamus controls homeostasis, metabolism, and reproductive functions through a variety of intricate interconnecting neural circuits. Previous studies suggested that coronet cells in the *Ciona* sensory vesicle correspond to a "proto-hypothalamus" and are homologous to dopaminergic neurons in the vertebrate hypothalamus (*13*, *14*). More recent studies show that coronet cells also have nondopaminergic neurosecretory activities, raising the possibility that cellular subfunctionalization produced multiple specialized cell types in the vertebrate hypothalamus (*15*).

Here, we compare the expression of key marker genes and single-cell whole-transcriptome profiles in the *Ciona* sensory vesicle and mouse hypothalamus. These studies suggest that coronet cells are not the only rudiment of the vertebrate hypothalamus. We present evidence for additional similarities, including switch neurons (mammillary nucleus), *FoxP*$^+$ relay neurons (RNs) (magnocellular neurons), and *VP*$^+$ and *VPR*$^+$ RNs (arcuate nucleus). These studies suggest that proto-vertebrates had a sophisticated hypothalamus with multiple cell types. We propose that a major function of the *Ciona* proto-hypothalamus is to trigger the onset of metamorphosis in response to twilight, similar to the regulation of photoperiodism by the saccus vasculosus of nontropical fishes.

RESULTS

Identification of *Ciona* sensory vesicle cell types

Single-cell transcriptome profiling of *Ciona intestinalis* embryogenesis, from gastrulation to swimming larvae, identified 40 *t*-distributed stochastic neighbor embedding (t-SNE) cell clusters comprising both the CNS and peripheral nervous system (*6*). In this study, we mapped each of the neural cell types comprising the simple brain, or sensory vesicle. The transcriptome profiles of each cell type identified marker genes that exhibit preferential expression in specific lineages. The regulatory regions of these markers were used to create reporter genes that are expressed in individual cell types (Fig. 1A, fig. S1A, and table S1). Together, these studies identified 15 different neural cell types (table S2). They include previously identified coronet cells, Eminens neurons, vasopressin/oxytocin-expressing RNs (*VP*$^+$), and pigment cells (figs. S2, A and B, and S3, A to C).

Neural-specific reporter genes identified a variety of RNs, including *FoxP*$^+$ RNs (Fig. 1B and fig. S2, C to E) that express vasopressin and tachykinin, as well as *VPR*$^+$ RNs, which express the vasopressin receptor (Fig. 1C and fig. S2, F and G). The *FoxP*$^+$ RNs are cholinergic, while the VPR$^+$ RNs are GABAergic [GABA (γ-aminobutyric acid) releasing]. We also mapped another small population of GABAergic RNs, *Mib*$^+$ (fig. S2, H and I), and GABAergic interneurons (INs) (Fig. 1D and fig. S2, J to N).

[1]Lewis-Sigler Institute for Integrative Genomics, Princeton University, Princeton, NJ, USA. [2]Department of Molecular Biology, Princeton University, Princeton, NJ, USA.
*Corresponding author. Email: msl2@princeton.edu
†These authors contributed equally to this work.
‡Present address: Department of Molecular and Cell Biology, University of California, Berkeley, Berkeley, CA, USA.
§Present address: WuXi AppTec, Shanghai, China.

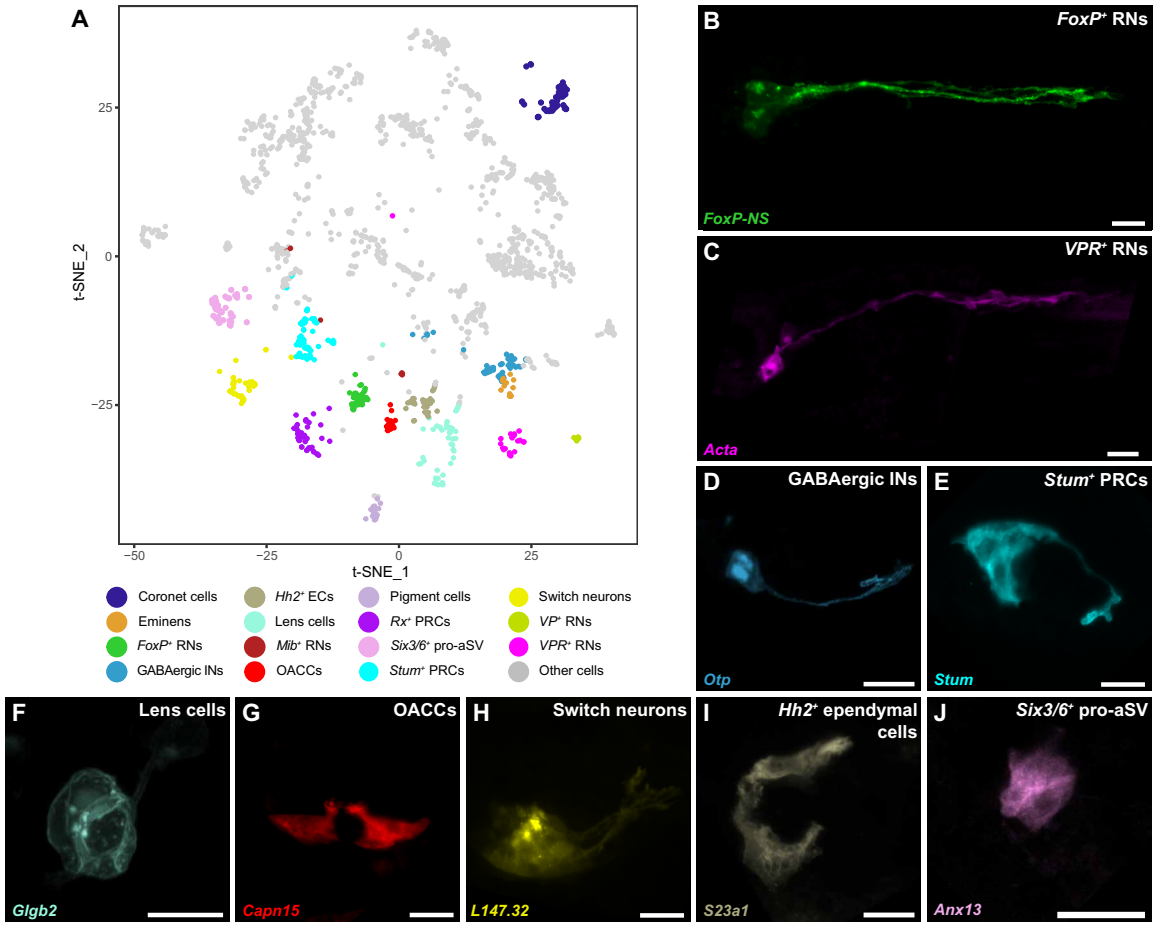

Fig. 1. Brain map. (**A**) t-SNE plot of the *Ciona* nervous system cells in swimming tadpoles ($n = 2021$ cells). The color-coded cells belong to cell types in the sensory vesicle. Gray cells correspond to cells outside of the sensory vesicle. The identification of the different clusters was determined at the larva stage by expression of membrane fluorescent reporters under the control of regulatory sequences for genes enriched in the cluster of interest: (**B**) *FoxP*$^+$ RNs expressing *FoxP* regulatory sequences specifically active in the nervous system (*FoxP*-NS reporter; green), (**C**) *VPR*$^+$ RNs (*Acta* reporter; magenta), (**D**) GABAergic INs (*Otp* reporter; blue), (**E**) *Stum*$^+$ PRCs (*Stum* reporter; cyan), (**F**) lens cells (*Glgb2* reporter; aqua), (**G**) the otolith associated ciliated cells (OACCs) (*Capn15* reporter; red), (**H**) switch neurons (*L147.32* reporter; yellow), (**I**) the *Hh2*$^+$ ependymal cells (ECs) (*S23a1* reporter; beige), and (**J**) the *Six3/6*$^+$ pro-anterior sensory vesicle (aSV) (*Anx13* reporter; pink). The description of the fusion genes used in the reporter assays and the number of replicates are provided in table S1. Scale bars, 10 μm.

Neural-specific reporter genes, along with previous connectome studies, allowed us to link single-cell transcriptome profiles to defined sensory cell types and associated accessory cells. Two distinct clusters of photoreceptor cells (PRCs), *Rx*$^+$ and *Stum*$^+$ subtypes (Fig. 1E and fig. S4, A to I), were identified along with associated accessory lens cells (Fig. 1F and fig. S3, G and H) (*16*–*18*). The *Rx*$^+$ PRCs correspond to most of the PRCs present in the three groups of PRCs (fig. S4, A to G). The otolith-associated ciliated cells, involved in gravity sensing, were also characterized. One of its marker genes, *Prod2*, is also strongly expressed in the antenna cells (Fig. 1G and fig. S3, I and J) (*16*, *19*).

Our studies also revealed an underappreciated population of putative mechanosensory neurons (*7*), renamed "switch neurons" (Fig. 1H and fig. S4, J to N). These neurons correspond to ciliated brain interneurons in the connectome map of the tadpole CNS (see below) (*7*, *20*). Furthermore, we identified the sensory vesicle ependymal cells as *Hh2*$^+$ (Fig. 1I and fig. S3, D to F). A subset of them are tightly associated with the gravity-sensing otolith (fig. S3, D to F). Lastly, the anteriormost cells of the sensory vesicle, *Six3/6*$^+$ pro-aSV cells, are likely to harbor motile cilia based on their transcriptome signatures (Fig. 1J and fig. S3K).

A putative coronet cell neuronal circuit

Previous studies highlighted similarities of coronet cells with the vertebrate hypothalamus because they release dopamine and express different neuropeptides such as neurotensin-like B and gonadotropin-releasing hormone (Gnrh) (*13*, *15*). However, they were first described as sharing morphological similarities with the coronet cells of the saccus vasculosus, a region of the hypothalamus seen in nontropical fishes (*16*, *21*, *22*). Fish coronet cells express melanopsin and detect short-wavelength light associated with seasonal lengthening of daylight, triggering reproduction via release of thyroid-stimulating hormone followed by secretion of Gnrh, as in other seasonal breeders (*23*–*25*).

Transcriptome profiling shows that *Ciona* coronet cells also express melanopsin. This was confirmed by attaching melanopsin regulatory sequences to a green fluorescent protein (GFP) reporter gene and coexpressing it along with a *Ptf1a* reporter that labels all

coronet cells (Fig. 2A and fig. S5A). They also express pinopsin, another opsin related to circadian rhythms (Fig. 2B and fig. S5B) (*26*). We therefore suggest that coronet cells function as light-sensing sensory cells, in addition to their dopaminergic and neurosecretory activities.

Coronet cells interact with several adjacent neurons, including switch neurons and *FoxP*$^+$ RNs (Fig. 2, C to G). Switch neurons are likely to receive dopaminergic inputs from coronet cells because they express two genes encoding *Adra2*, an adrenoreceptor that is able to bind dopamine with high affinity (Fig. 2, D and E, and fig. S4M) (*27*). On the basis of their position in the anterior sensory vesicle close to the otolith (Fig. 2C) and extensive associations with coronet cells, it is likely that switch neurons correspond to ciliated brain interneurons, which are postsynaptic to the coronet cells in the connectome (*7*, *20*).

On the basis of cell-cell associations, it is possible that the *VPR*$^+$ RNs receive inputs from switch neurons (fig. S5C). Moreover, the single-cell data support this hypothesis because the switch neurons are glutamatergic (fig. S4N), and the *VPR*$^+$ RNs express AMPA receptor (fig. S1B). They also appear to receive additional sensory inputs from both antenna cells (gravity) and group I and II PRCs (light), which are both glutamatergic (fig. S5, D and E) (*28*). Once again, the connectome identified synapses between coronet cells and adjacent RNs, most likely *FoxP*$^+$ neurons (Fig. 2, F and G). Neither *VP*$^+$ nor *VPR*$^+$ RNs have substantial cellular contacts with coronet cells (fig. S5F). However, the nature of coronet-*FoxP*$^+$ interactions is unclear because transcriptome trajectories indicate that *FoxP*$^+$ RNs do not express substantial levels of transcripts encoding dopaminergic receptors such as *Adra2* (fig. S1C). The *FoxP*$^+$ RNs would be able to modulate the activity of both the switch neurons and coronet cells through vasopressin/oxytocin signals neurons because they express a vasopressin receptor (fig. S1A).

NeuroD specifies mechanosensory switch neurons

The preceding analysis suggests that coronet cells might be a central sensory node for associated switch neurons and *FoxP*$^+$ RNs. While there is detailed information about the networks underlying the specification of coronet cells (*6*, *15*), little is known about the development of either switch neurons or *FoxP*$^+$ RNs. We chose to focus our efforts on switch neurons because they are evocative of a specialized mechanosensory cell type in vertebrates, the cerebrospinal fluid contacting neurons (CSF-cNs), which are present along the central canal and ventricular cavities of the brain including the hypothalamus (*29*, *30*). Like CSF-cNs (*31*, *32*), *Ciona* switch neurons express *Pkd2l* and extend cilia into the lumen of the sensory vesicle. In contrast, other neurons that express *Pkd2l*, such as *FoxP*$^+$ RNs or GABAergic INs, lack cilia (Fig. 2, H and I, and fig. S5, G to I). The presence of cilia in switch neurons is confirmed by their transcriptional signature because they expressed multiple genes involved in ciliogenesis such as *Ift88*, *Gels*, *Cep41*, *and Ptn23* (*33*–*36*). Moreover, switch neurons also express *Trpa1*, which transduces mechanosensation from *Caenorhabditis elegans* to vertebrates (*37*–*39*).

Not much is known about the development or function of vertebrate CSF-cNs. In an effort to gain insights into their ontogeny, we created a provisional gene regulatory network for switch neurons. The network was constructed using previously published methods (Materials and Methods). Namely, transcriptome trajectories and temporal cascades of genes encoding transcription factors were identified in the cell lineages forming switch neurons (Fig. 3, A and B). DNA recognition sequences for transcription factors that are expressed

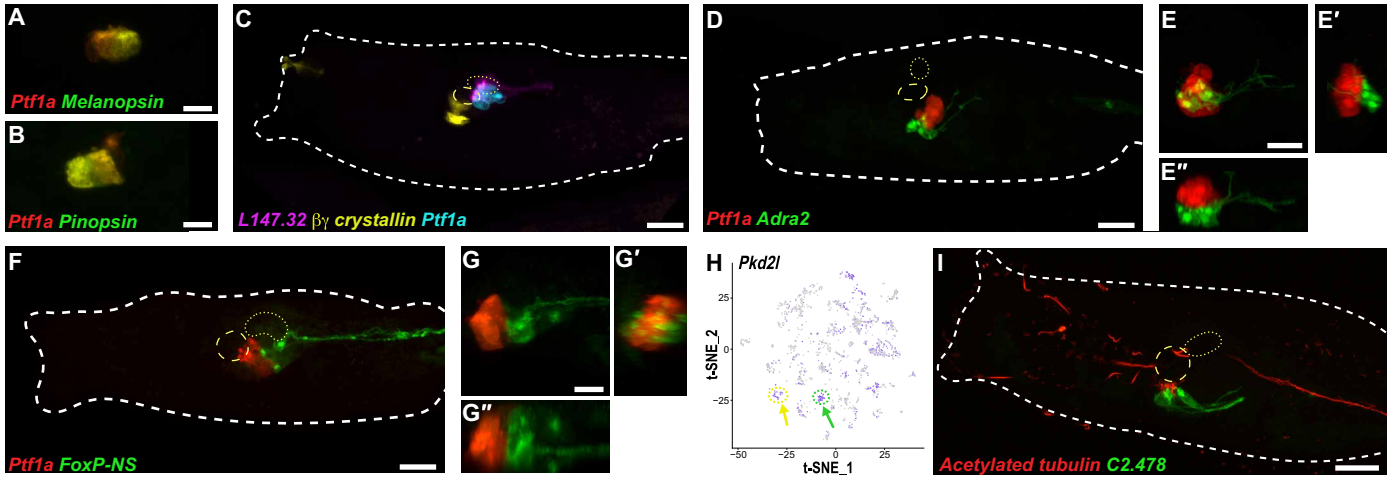

Fig. 2. Coronet-associated circuit in swimming tadpoles. (**A** and **B**) Expression of reporter genes for melanopsin [(A), green] or pinopsin [(B), green] and a *Ptf1a* reporter gene (red) in coronet cells. (**C**) Switch neurons (*L147.32* reporter; magenta) are closely associated with coronet cells (*Ptf1a* reporter; cyan) and the otolith (βγ-crystallin reporter; yellow) without touching the latter. (**D**) Coexpression of *Ptf1a* and *Adra2* reporter genes (red and green, respectively) also show close associations of switch neurons and coronet cells. (**E** to **E″**) Higher-magnification views of the reporter genes shown in (D). (E) is a *z*-projection, (E′) *y*-projection, and (E″) *x*-projection, which highlights extensive cell-cell contacts between switch neurons and coronet cells. (**F**) Expression of a *FoxP*$^+$ reporter gene (green) shows close contact of *FoxP*$^+$ RNs with coronet cells (*Ptf1a* reporter; red). (**G** to **G″**) Higher-magnification views of the reporter genes shown in (F), corresponding to *z*-, *y*-, and *x*-projections, respectively. (**H**) t-SNE plot of *Pkd2l* expression across the nervous system ($n = 2021$ cells). The yellow dotted circle and arrow indicate the switch neurons, while the green dotted circle and arrow point to the *FoxP*$^+$ RNs. (**I**) Immunostaining for acetylated tubulin (red) reveals cilia in switch neurons that were labeled with *C2.478* reporter (green). All reporter assays were analyzed at the larva stage. Reporter genes code for membrane fluorescent proteins and their description as well as the number of replicates are provided in table S1. White dashed lines indicate the outline of the trunk regions of tadpoles, while yellow dotted and dashed lines identify the pigment of the ocellus and the otolith, respectively. Scale bars, 10 μm (A, B, E, and G) and 20 μm (C, D, F, and I).

early in the lineage were identified in the 5′ regulatory regions of genes expressed at later stages. The resulting interconnections can be represented as a provisional gene network (Fig. 3C).

As an initial effort to test the authenticity of the network, we misexpressed *NeuroD* throughout the a-lineage (anterior neural plate) using the *Dmrt1* enhancer (*Dmrt1>NeuroD* transgene). *NeuroD* was selected for this analysis because it exhibits restricted expression in the switch lineage (Fig. 4A and fig. S6A). Previously, we have found that neural-specific transcription factors are effective predictors of cell identity. For example, misexpression of *Prop1* results in supernumerary Eminens neurons, while misexpression of *Ptf1a* produces additional coronet cells (*6*, *15*). Transgenic larvae expressing the *Dmrt1>NeuroD* transgene exhibit malformations of the sensory vesicle due to transformations of the anterior neural plate into supernumerary switch neurons (Fig. 4, B and C, and fig. S6B).

We used single-cell RNA sequencing (scRNA-seq) assays to identify the cell types that are transformed into switch neurons upon misexpression of *NeuroD* (Fig. 4D and fig. S6, C to E). These studies suggest that many derivatives of the a-lineage are transformed, but palp sensory cells and pigment cells display the highest losses in transgenic larvae, suggesting that they are most efficiently transformed into switch neurons. It is possible that efficient transformation of palp sensory cells reflects their similarities as mechanosensory cells (*40*). The pigment cell lineage (a8.25) was shown to be "plastic" and readily reprogrammed to form ectomesenchymal cells upon misexpression of *Twist* (*2*).

Orthology maps of the mouse hypothalamus and *Ciona* nervous system

We have provided evidence for a putative sensory circuit that features coronet cells as a central node, in association with switch mechanosensory neurons and *VPR*$^+$ and *FoxP*$^+$ RNs. Previous studies, along with the current demonstration that coronet cells express melanopsin and pinopsin, provide considerable evidence for homology with the vertebrate hypothalamus. However, what about the associated switch and RNs?

To determine whether they might also share homology with the hypothalamus, we have performed whole-transcriptome comparisons with single-cell datasets of the mouse hypothalamus. Single-cell transcriptomes for each of the 40 neural cell types comprising the *Ciona* nervous system were compared with transcriptome maps of the mouse hypothalamus (*41*) using shared orthologous genes that are conserved between the two species (Materials and Methods, figs. S7 to S10, and tables S3 and S4). These studies identified two *Ciona* lineages that match two different clusters of mouse hypothalamic cells. Switch neurons coincide with mouse cluster 12, which contains glutaminergic neurons that express *Lhx9* and *FoxP2* in the mammillary nucleus (Fig. 5A) [Romanov *et al.* (*41*)]. The sister lineages formed by the *VP*$^+$ and *VPR*$^+$ RNs (*VP*$^+$/*VPR*$^+$ RNs) coincide with cluster 29, containing *Agrp*$^+$ neurons of the arcuate nucleus (Fig. 5B) [Romanov *et al.* (*41*)].

Unsupervised clustering with mouse hypothalamic marker genes (Materials and Methods) lends additional support for homology of switch neurons with mouse cluster 12 (mammillary nucleus) and *VP*$^+$/*VPR*$^+$ RNs with mouse cluster 29 (*Agrp*$^+$ arcuate nucleus) (Fig. 5C). Moreover, *Ciona FoxP*$^+$ RNs express a variety of effector genes seen in magnocellular neurons of the hypothalamic supraoptic and periventricular nuclei, including vasopressin (*VP*), adenosine receptor (*Aa1r*), neurokinin B receptor (*Nk1r*), and tachykinin (fig. S1C) (*42*–*46*). Together, comparative transcriptome analyses suggest that the coronet-associated neural circuit contains multiple cell

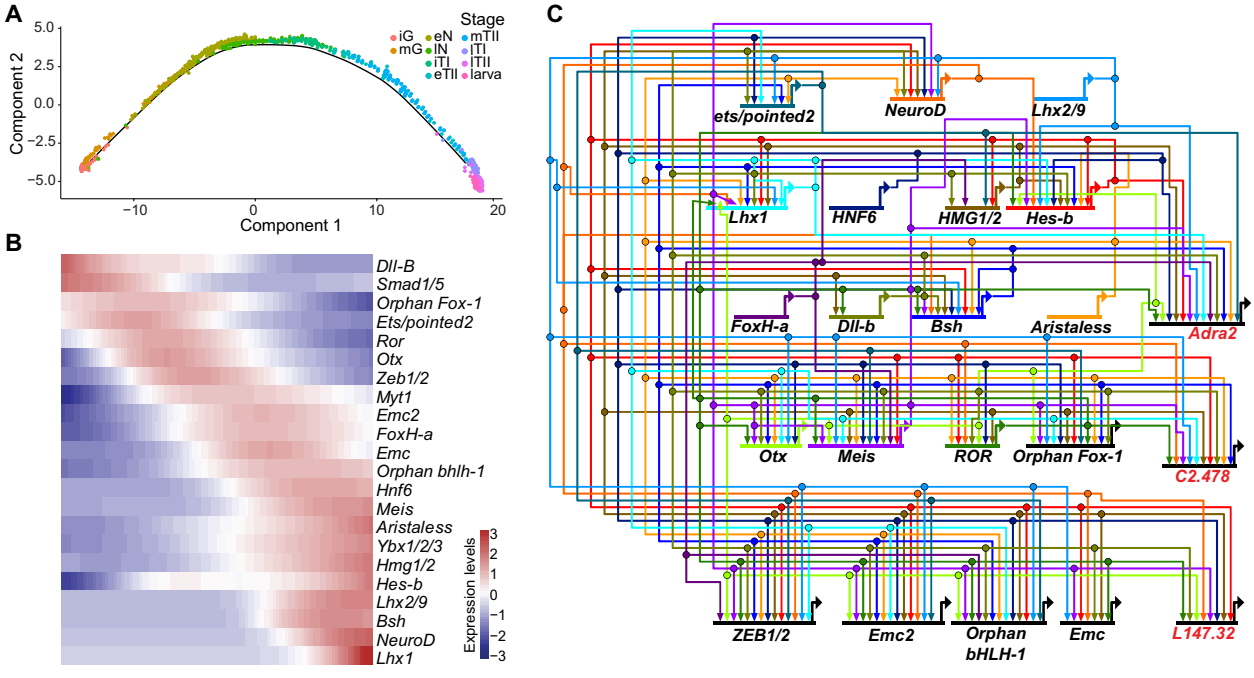

Fig. 3. Switch neuron provisional gene regulatory network. (**A**) Single-cell transcriptome trajectory of the switch neuron during development ($n = 1467$ cells). The cells are ordered on the basis of pseudo-time, and the color code indicates their stage. iG, initial gastrula; mG, mid gastrula; eN, early neurula; lN, late neurula; iTI, initial tailbud I; eTII, early tailbud II; mTII, mid tailbud II; lTI, late tailbud I; lTII, late tailbud II. (**B**) Pseudo-temporal gene expression cascade of switch neurons. Expression of representative transcription factors and signaling components in reconstructed developmental trajectories. (**C**) Provisional gene regulatory network of switch neurons based on the regulatory cascade (Materials and Methods).

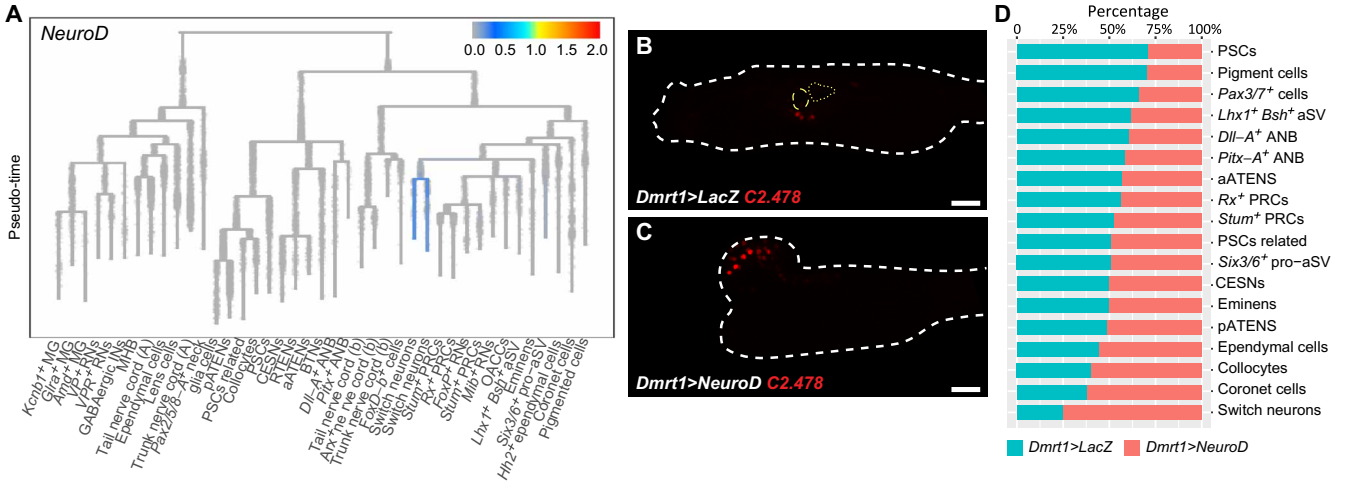

Fig. 4. *NeuroD* is a key determinant of the switch neuron lineage. (**A**) *NeuroD* expression along the virtual lineage tree of the *Ciona* nervous system ($n = 22{,}198$ cells). *NeuroD* is specifically expressed in the switch neuron lineages. (**B** and **C**) Overexpression of *NeuroD* in the anterior neural plate using a *Dmrt1>NeuroD* transgene results in the formation of supernumerary switch neurons detected with a nuclear reporter gene for *C2.478* [(C), red] as compared with control larvae (B). Transgene description and number of replicates are provided in table S1. White dashed lines outline trunk regions of larvae, while yellow dotted and dashed lines identify the pigment of the ocellus and the otolith, respectively. Scale bars, 20 μm. (**D**) scRNA-seq analysis of *NeuroD* overexpression. Percentage of cells within each a-lineage neural cell cluster upon *NeuroD* overexpression ($n = 3708$ cells) as compared with control late tailbud embryos ($n = 3256$ cells). aATENs, anterior apical trunk epidermal neurons; ANB, anterior neural boundary; BTNs, bipolar tail neurons; CESNs, caudal epithelial sensory neurons; MG, motor ganglion; MHB, midbrain-hindbrain boundary; pATENS, posterior apical trunk epidermal neurons; PSCs, palp sensory cells; RTENs, rostral trunk epidermal neurons.

types related to different regions of the mouse hypothalamus (summarized in Fig. 6).

DISCUSSION

Our studies identified 15 different cell types in the sensory vesicle of *Ciona* larvae (Fig. 6), whereas the connectome map identified 31 cell types (*7*, *20*). This twofold disparity is likely to reflect the different methods used for classification. It is easy to imagine that a single cell type based on intrinsic genetic properties can acquire distinctive behaviors through associations with different neurons. For example, we described five different types of RNs based on transcriptome trajectories and profiles, while the connectome map identified 11 such neuron types based on synaptic inputs. Additional studies will be necessary to obtain a comprehensive and integrated map of transcriptomic cell types and connectome.

The similarities of coronet cells and associated neurons in *Ciona* with different cell types in the vertebrate hypothalamus suggest that the simple brain of *Ciona* contains a complex proto-hypothalamus (Fig. 6). Previous studies identified coronet cells as a putative rudiment of the vertebrate hypothalamus. Here, we provided evidence for additional homologies, including switch neurons and three different RN lineages, $FoxP^+$, and the sister lineages VP^+ and VPR^+.

Transcriptome profiles and synaptic connectome maps suggest functional associations of proto-hypothalamic cell types. For example, coronet cells and switch neurons express dopaminergic pathway genes and adrenergic receptors, respectively. It is likely that they form chemical synapses on the basis of their location within the sensory vesicle and connectome. Our reporter assays and transcriptome profiles further suggest the presence of synapses between the axons of switch neuron axons and the VPR^+ RNs. Similarly, the connectome identified just a few synaptic inputs from coronet cells to RNs, probably adjacent $FoxP^+$ RNs (*7*). They might also communicate through vasopressin/oxytocin neuropeptides and a vasopressin receptor that are expressed by coronet cells and $FoxP^+$ neurons, respectively. What is the function of this intricate proto-hypothalamic neuronal circuit?

The ciliated switch neurons might be involved in mechanosensation. They express two voltage-dependent cation channels from the Trp family, *Pkd2l* and *Trpa1*. The first is associated with mechanosensation and pH sensing in the vertebrate CSF-cNs, while the other transduces thermosensation in invertebrates and mechanosensation in the inner ear (*37*, *39*). The likely function of switch neurons is to sense shear stress movements within the lumenal fluid of the sensory vesicle through their cilia. They could therefore help position the larva by detecting gravity in association with antenna cells and the otolith. However, the involvement of *Trpa1* in thermoregulation raises the possibility that switch neurons could also respond to changes in temperature, as well as gravity and mechanical cues.

While the primary role of the switch neurons would be to perceive mechanical cues, we propose that the coronet cells are involved in light sensation as previously suggested (*14*, *21*, *47*). The "coronet circuit" might detect short-wavelength light during twilight hours to help trigger the onset of metamorphosis. *Ciona* tadpoles swim in shallow ocean waters to disperse populations of sessile adults. At twilight, *Ciona* tadpoles undergo a behavioral switch. They no longer swim near the surface but instead "dive" into deeper, darker waters where they attach to hard surfaces and undergo metamorphosis (*48*, *49*). Recent studies have implicated the GABA-Gnrh axis in this process (*50*). However, the signal causing the switch in behavior from dispersion to diving has not been uncovered. We suggest that melanopsin and pinopsin expressed in coronet cells are involved in this process. Their activation during the dimming of the light could lead to the release of specific neurotransmitters and neuropeptides. A similar circuit appears to be used by coronet cells in salmon for the detection of lengthening daylight (photoperiodism) underlying seasonal reproduction (*23*). Moreover, daylength is also able to modulate dopamine synthesis in the mouse retina (*51*). In the case of the *Ciona* tadpole, it could

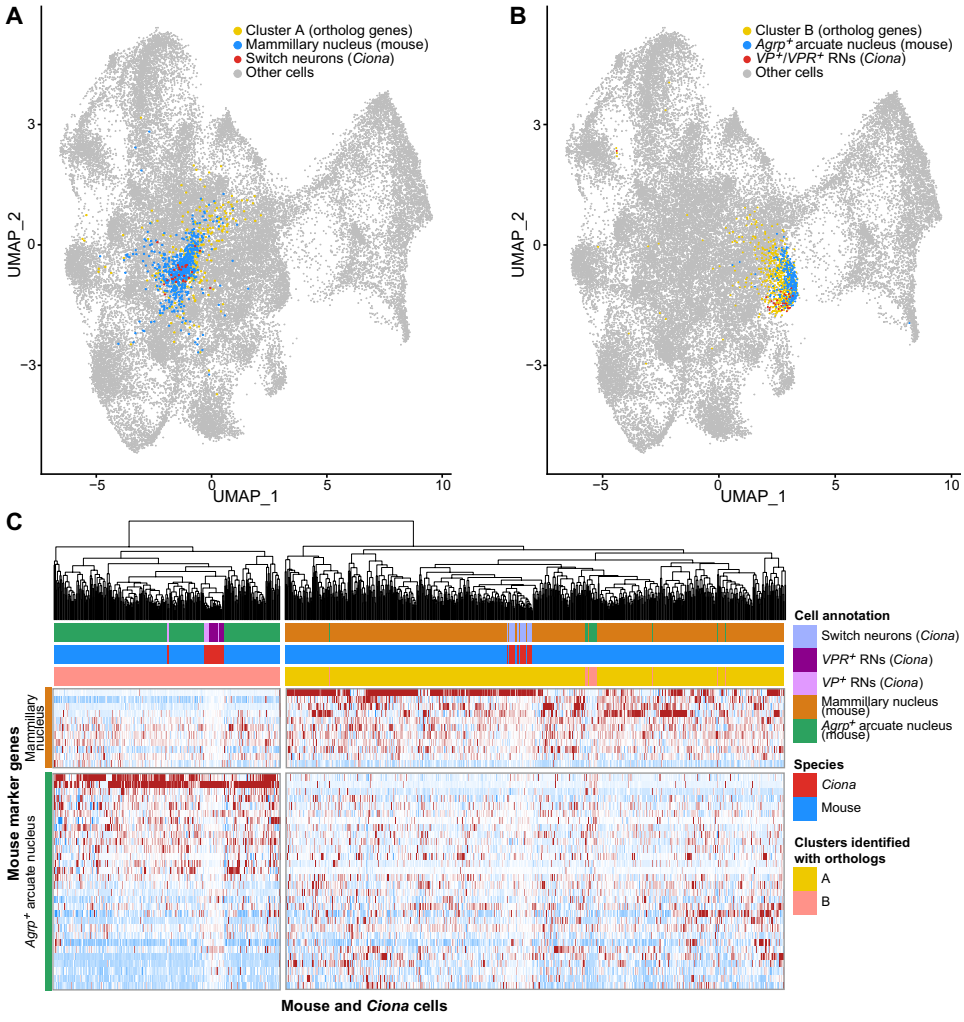

Fig. 5. Integration of mouse hypothalamus single-cell transcriptome with *Ciona* nervous system. (**A**) Uniform manifold approximation and projection (UMAP) showing the integrated coclustering of single-cell transcriptome datasets of the *Ciona* nervous system (late tailbud II and larva stage; $n = 4445$ cells) and mouse hypothalamus ($n = 33{,}893$ cells) based on shared orthologous genes. *Ciona* switch neurons and the mouse mammillary nucleus are colocalized in the same cluster. (**B**) Colocalization of *Ciona* VP^+ RNs, VPR^+ RNs, and mouse $Agrp^+$ arcuate nucleus cluster in the integrated data. (**C**) Heatmap of marker genes shared between mouse mammillary nucleus and $Agrp^+$ arcuate nucleus clusters and *Ciona* switch neurons and VP^+/VPR^+ RNs, respectively. Unsupervised clustering is consistent with orthology of *Ciona* switch neurons and mouse mammillary nucleus, and *Ciona* VP^+/VPR^+ RNs and mouse $Agrp^+$ arcuate nucleus.

modulate the activity of the switch neurons through dopamine secretion, which, in turn, activate the VPR^+ RNs leading to the secretion of GABA. Alternatively, coronet cells could alter swimming behavior by signaling $FoxP^+$ RNs. Moreover, the phenotype observed upon deletion of the proenzyme convertase *PC2* is more severe than *Gnrh* mutants (*50*), raising the possibility that coronet cells or its targets promote metamorphosis by secreting neuropeptides such as vasopressin/oxytocin, which has been shown to have a direct role in metamorphosis in some vertebrates (*52*).

Regardless of function, our evidence for multiple hypothalamic cell types in *Ciona* suggests that the apparently simple sensory vesicle has an unexpectedly sophisticated blueprint for the evolution of the complex vertebrate brain. Future studies will leverage the vast explosion of single-cell datasets to explore the origins of the neuronal cell types of different parts of the brain.

MATERIALS AND METHODS

Ciona handling, electroporation, and embryo collection

Adult *C. intestinalis* type A (Pacific species also named *Ciona robusta*) collected in the Pacific Ocean were purchased from M-Rep San Diego, CA and MarinUS, Long Beach, CA. The gametes were collected as previously described by Christiaen *et al.* (*53*). The electroporation of one-cell stage embryos with 20 to 100 μg of transgenic DNA was performed as previously described by Christiaen *et al.* (*54*). The embryos were reared at 18°C. For reporter assays, the embryos were fixed at the larva stage, 20 hours after fertilization, in MEM-FA [4% formaldehyde, 0.1 M Mops (pH 7.4), 0.5 M NaCl, 1 mM EGTA, 2 mM $MgSO_4$, and 0.05% Tween 20] for 30 min at room temperature, washed several times in PBT [phosphate-buffered saline (PBS) with 0.01% Tween 20], and mounted on slides using FluorSave Reagent (Millipore). The reporter assay experiments were performed at least in triplicate (table S1).

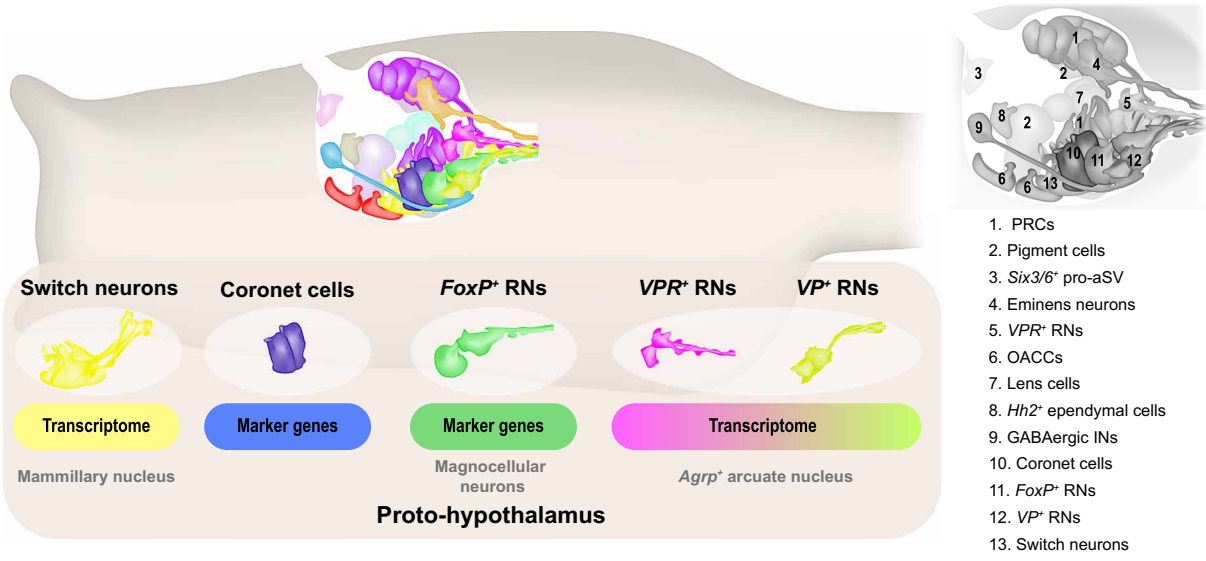

Fig. 6. The hypothalamus predates the origin of vertebrates. Fifteen different clusters were identified within the *Ciona* sensory vesicle. Coronet cells have been considered as a "rudimentary" hypothalamus owing to their expression of dopamine pathway genes and neuropeptide such as *Gnrh*. Additional neurons within the "coronet-associated circuit" also share similarities with different regions of the hypothalamus. *FoxP*$^+$ RNs express several genes that are evocative of magnocellular neurons of the supraoptic and periventricular nuclei of the hypothalamus. Comparative transcriptome analyses suggest orthology of switch neurons and the mouse mammillary nucleus, as well as *VP*$^+$/*VPR*$^+$ RNs and mouse *Agrp*$^+$ neurons in the arcuate nucleus. These observations suggest that several different hypothalamic cell types predate the vertebrate brain. The numbers on the gray image on the right indicate the position of the different cell types. For clarity, *Mib*$^+$ RNs and the *Stum*$^+$ PRCs have been omitted, and the number of cells of each type has also been reduced.

Cloning

The KH2012 gene model (KH ID) of the *C. intestinalis* type A genes mentioned in this article is listed in table S5. The regulatory sequences for βγ *crystallin*, *Dmrt1*, *Gad*, *NP*, *Opn1*, *Ptf1a*, *S39aa*, *vAcht*, and *Znt3* have been previously described (*2*, *6*, *55*–*58*). The regulatory sequence of *Aar1*, *Acta*, *Adra2*, *Anx13*, *C1.569*, *C2.1036*, *C2.478*, *Capn15*, *Fbn1*, *Glgb1*, *Glgb2*, *L147.32*, *Lhx2/9*, *Lmx1*, *Melanopsin*, *Otp*, *Prod2*, *S23a1*, *Stum*, *vGlut*, and *VPR* were polymerase chain reaction (PCR)–amplified from genomic DNA (gDNA) (primers in table S6). Regulatory sequences were cloned by either recombination or ligation (NEBuilder, New England Biolabs; T4 DNA ligase, Promega, respectively) into the pCESA reporter constructs driving the expression of a fluorescent protein targeted to the membrane by a palmitoylation signal (CAAX) or by the plekstrin homology (PH) domain of human PLCδ1 (CFPCAAX, GFPCAAX, mCherryCAAX, mAppleCAAX, neonGreen:PH, and YFPCAAX) or fused to a histone protein (H2B:GFP, H2B:mApple, or H2B:mCherry) (see tables S1 and S6) (*6*, *58*). After amplification from gDNA (table S6), *FoxP*, *Pinopsin*, and *Piwi* were cloned upstream of the minimal fog promoter driving the expression of membrane targeted GFP or yellow fluorescent protein (YFP) (GFPCAAX or YFPCAAX). After PCR amplification from complementary DNA (cDNA) of mid-tailbud embryos (table S6), *NeuroD* coding sequence was cloned into a pCESA vector downstream of the regulatory sequences of *Dmrt1*. *Dmrt1* driving the expression of LacZ was previously described (*58*).

Immunostaining

The immunostaining assay protocol was modified from the study by Wagner and Levine (*58*). In brief, the larvae were fixed at 20 or 24 hours after fertilization in MEM-FA. After washes in PBT, pretreatment in PBS with 0.1% Triton, washes in PBT, and incubation for 30 min in blocking solution at room temperature [10% Western blocking solution (Sigma-Aldrich) in PBT], the larvae were incubated at 4°C overnight with anti–acetylated tubulin antibody (1:500; Sigma-Aldrich, T7451) in blocking solution. After washes in PBT, the primary antibody was detected using goat anti-mouse antibody conjugated to Alexa Fluor 555 (1:1000; Thermo Fisher Scientific, A21424) diluted in blocking solution for 45 min at room temperature. The larvae were washed several times in PBT and mounted on slides using FluorSave Reagent (Millipore).

Image acquisition and quantification

The images were acquired with a Zeiss 880 confocal microscope with or without the super-resolution module (Airyscan, high-magnification images). Images acquired with the Airyscan module were processed using the default settings. For *NeuroD* overexpression experiments, one-cell stage embryos were electroprated with *C2.478>H2B:mCherry* and *Dmrt1>NeuroD* or *C2.478>H2B:mCherry* and *Dmrt1>LacZ*. Quantification of the number of *C2.478*$^+$ cells (H2B:mCherry$^+$ cells) at the larva stage was performed on sum-projected confocal images, and embryos from three electroporations were pooled into *NeuroD* overexpression and control conditions. The statistical significance was tested with Mann-Whitney test.

NeuroD overexpression and scRNA-seq

After fertilization using gametes from the same individual, one-cell stage embryos were electroporated with *Dmrt1>H2B:GFP* and *Dmrt1>LacZ* (control condition) or *Dmrt1>H2B:GFP* and *Dmrt1>NeuroD* (*NeuroD* overexpression condition). At the late tailbud stage I, morphologically normal embryos were selected, and at late tailbud II, GFP$^+$ embryos were dissociated as previously described by Cao *et al.* (*6*). The dissociation was performed in duplicate. The

cell concentration of each sample was checked by TC20 Automated Cell Counter to ensure that it was within 1000 to 2000 cells per microliter. Single-cell suspensions were loaded onto The Chromium Controller (10x Genomics). For all the samples, cells were lysed, and cDNAs were barcoded and amplified with the Chromium Single Cell 3′ Library and Gel Bead Kit v3 (10x Genomics) following the instructions of the manufacturer. Illumina sequencing libraries were prepared from the cDNA samples using the Nextera DNA library prep kit (Illumina). All the libraries were sequenced on Illumina NovaSeq 6000 with an S1 reagent kit (300 cycles, paired-end) following standard Illumina protocols. Raw sequencing reads were filtered by Illumina NovaSeq Control Software, and only pass-filtered reads were used for further analysis. Reads that aligned to phix (using Bowtie version 1.1.1) were removed, as were reads that failed Illumina's default chastity filter. We then combined the FASTQ files from each lane and separated the samples using the barcode sequences allowing one mismatch (using barcode_splitter version 0.18.2). In the read 2 of each sample, the rightmost bases after to position 100 were trimmed to keep only high-quality reads. Using 10x Cell Ranger version 3.0.2, the count pipeline was run with default settings on the trimmed FASTQ files to generate gene-barcode matrices for each sample. The reference sequence of *C. intestinalis* was obtained from the Ghost database (KH model 2012). The integration of scRNA-seq data of *NeuroD*-overexpressed embryos and the control embryos was performed with Seurat v3.0 (*59*).

Gene expression cascade and regulatory network

Switch neurons and their progenitor cells from initial gastrulation to larva stage were obtained from reconstructed single-cell trajectories of Arx^{+} pro-aSV and $Aristaless^{+}$ aSV, which were described by Cao *et al.* (*6*). We used monocle 2 to recover the single-cell trajectory of switch neurons. Highly variable regulatory genes and signaling pathway genes with $q < 1 \times 10^{-180}$ are shown in the pseudotemporal expression pattern in Fig. 3B, and cluster-buster (*60*) was used to investigate the putative direct interaction by searching clusters of prespecified motifs 2 kb upstream of the transcription start site of each gene. The parameters were set as follows: $g = 35$, $m = 4$, $c = 3$, score ≥ 4. The position frequency matrix was downloaded from the JASPAR 2018 database (*61*). Genes with no position frequency matrix recorded in JASPAR were not considered in constructing the regulatory network. The regulatory network in Fig. 3C was plotted with BioTapestry. Each line between two genes represents a putative direct interaction, as the binding motif of the regulatory gene was identified in the motif-cluster region of the target gene.

Integration of *Ciona* nervous system and mouse hypothalamus data

scRNA-seq data and cell type annotation of *Ciona* nervous system at late tailbud II and larva stages were obtained from the study by Cao *et al.* (*6*). The mouse hypothalamus data of E15 (embryonic day 15), E17, P0 (postnatal day 0), P2, P10, P23, and cell type annotation were obtained from the study by Romanov *et al.* (*41*). Orthologs and orthogroups between *Ciona* (KH2012) and mouse (mm10) were identified with OrthoFinder v2.3.12. In total, 18,218 orthogroups were found, and 5663 of them contain genes from both species. For each sample, orthogroup-barcode matrices were generated by keeping single-copy orthologs and summing one-to-many/many-to-one/many-to-many orthologs within the same orthogroups in *Ciona* and mouse, respectively. The clustering resolution with genes or orthogroups in *Ciona* and mouse was compared in figs. S7 and S8. In figs. S7 and S8, the data integration of *Ciona* or mouse orthogroup-barcode matrices was performed with log normalization and variable features identification followed by anchor integrations as described in Seurat v3.0 (*62*). In Fig. 5 and fig. S9, the data integration of mouse and *Ciona* orthogroup-barcode matrices was performed with SCTransform normalization and Pearson residual calculation. Clustering and UMAP visualization were performed with default parameters in Seurat v3.0 (clustering resolution is set to 3). In each identified cluster of integrated mouse and *Ciona* orthogroup-barcode matrices, the percentage of each cell type in *Ciona (6)* and in mouse (*41*) was calculated and demonstrated as a heatmap in fig. S10. The heatmap was plotted with pheatmap v1.0.10, and the distance of clustering metric was calculated with the "manhattan" method. Cell types that were distributed in more than 90% of the clusters identified by orthogroups were not included in the percentage calculation, as the orthogroups were not able to capture the characteristics of these cell types. Cluster 11 in mouse hypothalamus was deleted with this criterion.

SUPPLEMENTARY MATERIALS

Supplementary material for this article is available at http://advances.sciencemag.org/cgi/content/full/7/18/eabf7452/DC1

REFERENCES AND NOTES

1. S. M. Shimeld, A. G. Purkiss, R. P. Dirks, O. A. Bateman, C. Slingsby, N. H. Lubsen, Urochordate βγ-crystallin and the evolutionary origin of the vertebrate eye lens. *Curr. Biol.* **15**, 1684–1689 (2005).
2. P. B. Abitua, E. Wagner, I. A. Navarrete, M. Levine, Identification of a rudimentary neural crest in a non-vertebrate chordate. *Nature* **492**, 104–107 (2012).
3. P. B. Abitua, T. B. Gainous, A. N. Kaczmarczyk, C. J. Winchell, C. Hudson, K. Kamata, M. Nakagawa, M. Tsuda, T. G. Kusakabe, M. Levine, The pre-vertebrate origins of neurogenic placodes. *Nature* **524**, 462–465 (2015).
4. A. Stolfi, K. Ryan, I. A. Meinertzhagen, L. Christiaen, Migratory neuronal progenitors arise from the neural plate borders in tunicates. *Nature* **527**, 371–374 (2015).
5. R. Horie, A. Hazbun, K. Chen, C. Cao, M. Levine, T. Horie, Shared evolutionary origin of vertebrate neural crest and cranial placodes. *Nature* **560**, 228–232 (2018).
6. C. Cao, L. A. Lemaire, W. Wang, P. H. Yoon, Y. A. Choi, L. R. Parsons, J. C. Matese, M. Levine, K. Chen, Comprehensive single-cell transcriptome lineages of a proto-vertebrate. *Nature* **571**, 349–354 (2019).
7. K. Ryan, Z. Lu, I. A. Meinertzhagen, The CNS connectome of a tadpole larva of. *eLife* **5**, e16962 (2016).
8. D. Nicol, I. A. Meinertzhagen, Cell counts and maps in the larval central nervous system of the ascidian Ciona intestinalis (L.). *J. Comp. Neurol.* **309**, 415–429 (1991).
9. S. A. Sower, M. Freamat, S. I. Kavanaugh, The origins of the vertebrate hypothalamic-pituitary-gonadal (HPG) and hypothalamic-pituitary-thyroid (HPT) endocrine systems: New insights from lampreys. *Gen. Comp. Endocrinol.* **161**, 20–29 (2009).
10. M. Nozaki, Hypothalamic-pituitary-gonadal endocrine system in the hagfish. *Front. Endocrinol. (Lausanne)* **4**, 200 (2013).
11. D. Norris, J. Carr, *Vertebrate Endocrinology* (Academic Press, ed. 5, 2013).
12. B. Albuixech-Crespo, C. Herrera-Úbeda, G. Marfany, M. Irimia, J. Garcia-Fernàndez, Origin and evolution of the chordate central nervous system: insights from amphioxus genoarchitecture. *Int. J. Dev. Biol.* **61**, 655–664 (2017).
13. F. Moret, L. Christiaen, C. Deyts, M. Blin, J. S. Joly, P. Vernier, The dopamine-synthesizing cells in the swimming larva of the tunicate Ciona intestinalis are located only in the hypothalamus-related domain of the sensory vesicle. *Eur. J. Neurosci.* **21**, 3043–3055 (2005).
14. F. Razy-Krajka, E. R. Brown, T. Horie, J. Callebert, Y. Sasakura, J. S. Joly, T. G. Kusakabe, P. Vernier, Monoaminergic modulation of photoreception in ascidian: Evidence for a proto-hypothalamo-retinal territory. *BMC Biol.* **10**, 45 (2012).
15. T. Horie, R. Horie, K. Chen, C. Cao, M. Nakagawa, T. G. Kusakabe, N. Satoh, Y. Sasakura, M. Levine, Regulatory cocktail for dopaminergic neurons in a protovertebrate identified by whole-embryo single-cell transcriptomics. *Genes Dev.* **32**, 1297–1302 (2018).
16. R. M. Eakin, A. Kuda, Ultrastructure of sensory receptors in Ascidian tadpoles. *Z. Zellforsch. Mikrosk. Anat.* **112**, 287–312 (1971).
17. R. M. Eakin, A. Kuda, Glycogen in lens of tunicate tadpole (Chordata: Ascidiacea). *J. Exp. Zool.* **180**, 267–270 (1972).

18. T. Horie, D. Sakurai, H. Ohtsuki, A. Terakita, Y. Shichida, J. Usukura, T. Kusakabe, M. Tsuda, Pigmented and nonpigmented ocelli in the brain vesicle of the ascidian larva. *J. Comp. Neurol.* **509**, 88–102 (2008).
19. J. H. Imai, I. A. Meinertzhagen, Neurons of the ascidian larval nervous system in Ciona intestinalis: I. Central nervous system. *J. Comp. Neurol.* **501**, 316–334 (2007).
20. K. Ryan, I. A. Meinertzhagen, Neuronal identity: the neuron types of a simple chordate sibling, the tadpole larva of Ciona intestinalis. *Curr. Opin. Neurobiol.* **56**, 47–60 (2019).
21. P. N. Dilly, Studies on the receptors in Ciona intestinalis. 3. A second type of photoreceptor in the tadpole larva of Ciona intestinalis. *Z. Zellforsch. Mikrosk. Anat.* **96**, 63–65 (1969).
22. M. Benjamin, Ultrastructural studies on the coronet cells of the saccus vasculosus of the freshwater stickleback, Gasterosteus aculeatus form leiurus, Gasterosteus aculeatus form leiurus. *Z. Zellforsch. Mikrosk. Anat.* **147**, 551–565 (1974).
23. Y. Nakane, K. Ikegami, M. Iigo, H. Ono, K. Takeda, D. Takahashi, M. Uesaka, M. Kimijima, R. Hashimoto, N. Arai, T. Suga, K. Kosuge, T. Abe, R. Maeda, T. Senga, N. Amiya, T. Azuma, M. Amano, H. Abe, N. Yamamoto, T. Yoshimura, The saccus vasculosus of fish is a sensor of seasonal changes in day length. *Nat. Commun.* **4**, 2108 (2013).
24. T. Yamamura, K. Hirunagi, S. Ebihara, T. Yoshimura, Seasonal morphological changes in the neuro-glial interaction between gonadotropin-releasing hormone nerve terminals and glial endfeet in Japanese quail. *Endocrinology* **145**, 4264–4267 (2004).
25. T. Yoshimura, S. Yasuo, M. Watanabe, M. Iigo, T. Yamamura, K. Hirunagi, S. Ebihara, Light-induced hormone conversion of T4 to T3 regulates photoperiodic response of gonads in birds. *Nature* **426**, 178–181 (2003).
26. T. Kasahara, T. Okano, T. Haga, Y. Fukada, Opsin-G11-mediated signaling pathway for photic entrainment of the chicken pineal circadian clock. *J. Neurosci.* **22**, 7321–7325 (2002).
27. M. Sánchez-Soto, V. Casadó-Anguera, H. Yano, B. J. Bender, N. S. Cai, E. Moreno, E. I. Canela, A. Cortés, J. Meiler, V. Casadó, S. Ferré, α 2A - and α 2C -adrenoceptors as potential targets for dopamine and dopamine receptor ligands. *Mol. Neurobiol.* **55**, 8438–8454 (2018).
28. T. Horie, T. Kusakabe, M. Tsuda, Glutamatergic networks in the Ciona intestinalis larva. *J. Comp. Neurol.* **508**, 249–263 (2008).
29. B. Vigh, I. Vigh-Teichmann, Comparative ultrastructure of the cerebrospinal fluid-contacting neurons. *Int. Rev. Cytol.* **35**, 189–251 (1973).
30. J. R. Sternberg, A. E. Prendergast, L. Brosse, Y. Cantaut-Belarif, O. Thouvenin, A. Orts-Del'Immagine, L. Castillo, L. Djenoune, S. Kurisu, J. R. McDearmid, P. L. Bardet, C. Boccara, H. Okamoto, P. Delmas, C. Wyart, Pkd2l1 is required for mechanoception in cerebrospinal fluid-contacting neurons and maintenance of spine curvature. *Nat. Commun.* **9**, 3804 (2018).
31. L. Djenoune, H. Khabou, F. Joubert, F. B. Quan, S. Nunes Figueiredo, L. Bodineau, F. Del Bene, C. Burcklé, H. Tostivint, C. Wyart, Investigation of spinal cerebrospinal fluid-contacting neurons expressing PKD2L1: Evidence for a conserved system from fish to primates. *Front. Neuroanat.* **8**, 26 (2014).
32. A. L. Huang, X. Chen, M. A. Hoon, J. Chandrashekar, W. Guo, D. Tränkner, N. J. Ryba, C. S. Zuker, The cells and logic for mammalian sour taste detection. *Nature* **442**, 934–938 (2006).
33. G. J. Pazour, B. L. Dickert, Y. Vucica, E. S. Seeley, J. L. Rosenbaum, G. B. Witman, D. G. Cole, Chlamydomonas IFT88 and its mouse homologue, polycystic kidney disease gene tg737, are required for assembly of cilia and flagella. *J. Cell Biol.* **151**, 709–718 (2000).
34. P. Mburu, M. R. Romero, H. Hilton, A. Parker, S. Townsend, Y. Kikkawa, S. D. Brown, Gelsolin plays a role in the actin polymerization complex of hair cell stereocilia. *PLOS ONE* **5**, e11627 (2010).
35. J. E. Lee, J. L. Silhavy, M. S. Zaki, J. Schroth, S. L. Bielas, S. E. Marsh, J. Olvera, F. Brancati, M. Iannicelli, K. Ikegami, A. M. Schlossman, B. Merriman, T. Attié-Bitach, C. V. Logan, I. A. Glass, A. Cluckey, C. M. Louie, J. H. Lee, H. R. Raynes, I. Rapin, I. P. Castroviejo, M. Setou, C. Barbot, E. Boltshauser, S. F. Nelson, F. Hildebrandt, C. A. Johnson, D. A. Doherty, E. M. Valente, J. G. Gleeson, CEP41 is mutated in Joubert syndrome and is required for tubulin glutamylation at the cilium. *Nat. Genet.* **44**, 193–199 (2012).
36. J. Kim, J. E. Lee, S. Heynen-Genel, E. Suyama, K. Ono, K. Lee, T. Ideker, P. Aza-Blanc, J. G. Gleeson, Functional genomic screen for modulators of ciliogenesis and cilium length. *Nature* **464**, 1048–1051 (2010).
37. D. P. Corey, J. García-Añoveros, J. R. Holt, K. Y. Kwan, S.-Y. Lin, M. A. Vollrath, A. Amalfitano, E. L.-M. Cheung, B. H. Derfler, A. Duggan, G. S. G. Géléoc, P. A. Gray, M. P. Hoffman, H. L. Rehm, D. Tamasauskas, D.-S. Zhang, TRPA1 is a candidate for the mechanosensitive transduction channel of vertebrate hair cells. *Nature* **432**, 723–730 (2004).
38. K. Y. Kwan, A. J. Allchorne, M. A. Vollrath, A. P. Christensen, D.-S. Zhang, C. J. Woolf, D. P. Corey, TRPA1 contributes to cold, mechanical, and chemical nociception but is not essential for hair-cell transduction. *Neuron* **50**, 277–289 (2006).
39. K. S. Kindt, V. Viswanath, L. Macpherson, K. Quast, H. Hu, A. Patapoutian, W. R. Schafer, *Caenorhabditis elegans* TRPA-1 functions in mechanosensation. *Nat. Neurosci.* **10**, 568–577 (2007).
40. F. Zeng, J. Wunderer, W. Salvenmoser, M. W. Hess, P. Ladurner, U. Rothbächer, Papillae revisited and the nature of the adhesive secreting collocytes. *Dev. Biol.* **448**, 183–198 (2019).
41. R. A. Romanov, E. O. Tretiakov, M. E. Kastriti, M. Zupancic, M. Häring, S. Korchynska, K. Popadin, M. Benevento, P. Rebernik, F. Lallemend, K. Nishimori, F. Clotman, W. D. Andrews, J. G. Parnavelas, M. Farlik, C. Bock, I. Adameyko, T. Hökfelt, E. Keimpema, T. Harkany, Molecular design of hypothalamus development. *Nature* **582**, 246–252 (2020).
42. F. Vandesande, K. Dierickx, Identification of the vasopressin producing and of the oxytocin producing neurons in the hypothalamic magnocellular neurosecretroy system of the rat. *Cell Tissue Res.* **164**, 153–162 (1975).
43. T. A. Ponzio, G. I. Hatton, Adenosine postsynaptically modulates supraoptic neuronal excitability. *J. Neurophysiol.* **93**, 535–547 (2005).
44. S. H. Oliet, D. A. Poulain, Adenosine-induced presynaptic inhibition of IPSCs and EPSCs in rat hypothalamic supraoptic nucleus neurones. *J. Physiol.* **520** (Pt. 3), 815–825 (1999).
45. T. Hatae, H. Kawano, V. Karpitskiy, J. E. Krause, S. Masuko, Arginine-vasopressin neurons in the rat hypothalamus produce neurokinin B and co-express the tachykinin NK-3 receptor and angiotensin II type 1 receptor. *Arch. Histol. Cytol.* **64**, 37–44 (2001).
46. F. Marsais, A. Calas, Ectopic expression of non-catecholaminergic tyrosine hydroxylase in rat hypothalamic magnocellular neurons. *Neuroscience* **94**, 151–161 (1999).
47. S. Sharma, W. Wang, A. Stolfi, Single-cell transcriptome profiling of the Ciona larval brain. *Dev. Biol.* **448**, 226–236 (2019).
48. C. Grave, Amaroucium pellucidum (Leidy) form constellatum (Verrill). I. The activities and reactions of the tadpole larva. *J. Exp. Zool.* **30**, 239–257 (1920).
49. S. Kajiwara, M. Yoshida, Changes in behavior and ocellar structure during the larval life of solitary ascidians. *Biol. Bull.* **169**, 565–577 (1985).
50. A. Hozumi, S. Matsunobu, K. Mita, N. Treen, T. Sugihara, T. Horie, T. Sakuma, T. Yamamoto, A. Shiraishi, M. Hamada, N. Satoh, K. Sakurai, H. Satake, Y. Sasakura, GABA-induced GnRH release triggers chordate metamorphosis. *Curr. Biol.* **30**, 1555–1561.e4 (2020).
51. K. Okimura, Y. Nakane, T. Nishiwaki-Ohkawa, T. Yoshimura, Photoperiodic regulation of dopamine signaling regulates seasonal changes in retinal photosensitivity in mice. *Sci. Rep.* **11**, 1843 (2021).
52. J. E. Platt, M. J. LiCause, Effects of oxytocin in larval *Ambystoma tigrinum*: Acceleration of induced metamorphosis and inhibition of the antimetamorphic action of prolactin. *Gen. Comp. Endocrinol.* **41**, 84–91 (1980).
53. L. Christiaen, E. Wagner, W. Shi, M. Levine, Isolation of sea squirt (Ciona) gametes, fertilization, dechorionation, and development. *Cold Spring Harb. Protoc.* **2009**, pdb. prot5344 (2009).
54. L. Christiaen, E. Wagner, W. Shi, M. Levine, Electroporation of transgenic DNAs in the sea squirt Ciona. *Cold Spring Harb. Protoc.* **2009**, pdb.prot5345 (2009).
55. R. Yoshida, D. Sakurai, T. Horie, I. Kawakami, M. Tsuda, T. Kusakabe, Identification of neuron-specific promoters in Ciona intestinalis. *Genesis* **39**, 130–140 (2004).
56. T. Kusakabe, R. Yoshida, Y. Ikeda, M. Tsuda, Computational discovery of DNA motifs associated with cell type-specific gene expression in Ciona. *Dev. Biol.* **276**, 563–580 (2004).
57. K. Takamura, N. Minamida, S. Okabe, Neural map of the larval central nervous system in the ascidian *Ciona intestinalis*. *Zoolog. Sci.* **27**, 191–203 (2010).
58. E. Wagner, M. Levine, FGF signaling establishes the anterior border of the Ciona neural tube. *Development* **139**, 2351–2359 (2012).
59. A. Butler, P. Hoffman, P. Smibert, E. Papalexi, R. Satija, Integrating single-cell transcriptomic data across different conditions, technologies, and species. *Nat. Biotechnol.* **36**, 411–420 (2018).
60. M. C. Frith, M. C. Li, Z. Weng, Cluster-Buster: Finding dense clusters of motifs in DNA sequences. *Nucleic Acids Res.* **31**, 3666–3668 (2003).
61. A. Khan, O. Fornes, A. Stigliani, M. Gheorghe, J. A. Castro-Mondragon, R. van der Lee, A. Bessy, J. Chèneby, S. R. Kulkarni, G. Tan, D. Baranasic, D. J. Arenillas, A. Sandelin, K. Vandepoele, B. Lenhard, B. Ballester, W. W. Wasserman, F. Parcy, A. Mathelier, JASPAR 2018: Update of the open-access database of transcription factor binding profiles and its web framework. *Nucleic Acids Res.* **46**, D1284 (2018).
62. T. Stuart, A. Butler, P. Hoffman, C. Hafemeister, E. Papalexi, W. M. Mauck III, Y. Hao, M. Stoeckius, P. Smibert, R. Satija, Comprehensive integration of single-cell data. *Cell* **177**, 1888–1902.e21 (2019).

Acknowledgments: We thank the members of the Levine laboratory for helpful discussion especially A. Mariossi and N. Treen. We also thank J. Corbo from the Washington University School of Medicine in St. Louis, K. Ryan from the Dalhousie University, and R. Romanov from the Medical University of Vienna for insightful discussion. We also thank for technical support the Genomics Core Facility of the Lewis Sigler Institute for Integrative Genomics, W. Wang, J. B. Wiggins, and J. M. Miller, as well as L. R. Parsons from the Bioinformatics Office of the Lewis Sigler Institute for Integrative Genomics. **Funding:** This study was funded by a grant from the NIH (NS076542). **Author contributions:** L.A.L., C.C., and M.L. conceived the project. L.A.L., C.C., P.H.Y., and J.L. designed the experiments. L.A.L., P.H.Y., and J.L. performed the experiments.

C.C. performed the computational data analysis. All authors contributed to the interpretation of the results. L.A.L., C.C., and M.L. wrote the manuscript. **Competing interests:** The authors declare that they have no competing interests. **Data and materials availability:** All data needed to evaluate the conclusions in the paper are present in the paper and/or the Supplementary Materials. Data related to this paper are available upon request to M.L. The raw sequencing data and gene expression matrices are available in GEO (https://www.ncbi.nlm.nih.gov/geo/query/acc.cgi?acc=GSE166235) under the accession number: GSE166235.

Submitted 16 November 2020
Accepted 9 March 2021
Published 28 April 2021
10.1126/sciadv.abf7452

Citation: L. A. Lemaire, C. Cao, P. H. Yoon, J. Long, M. Levine, The hypothalamus predates the origin of vertebrates. *Sci. Adv.* **7**, eabf7452 (2021).

The hypothalamus predates the origin of vertebrates

Laurence A. Lemaire, Chen Cao, Peter H. Yoon, Juanjuan Long and Michael Levine

Sci Adv **7** (18), eabf7452.
DOI: 10.1126/sciadv.abf7452